JOURNAL OF MATERIALS RESEARCH AND TECHNOLOGY 2023;25:6865–6879

Available online at www.sciencedirect.com

jmr&t Journal of Materials Research and Technology

journal homepage: www.elsevier.com/locate/jmrt

Mechanism of material removal in tungsten carbide-cobalt alloy during chemistry enhanced shear thickening polishing

Jiahuan Wang [a,b,c], *Zewei Tang* [a,b], *Saurav Goel* [c,d], *Yu Zhou* [a,b], *Yanfei Dai* [a,b], *Jinhu Wang* [a,b], *Qiankun He* [a,b], *Julong Yuan* [a,b], *Binghai Lyu* [a,b,*]

[a] *College of Mechanical Engineering, Zhejiang University of Technology, Hangzhou, 310000, China*
[b] *Ultra-precision Machining Center, Key Laboratory of Special Purpose Equipment and Advanced Manufacturing Technology, Zhejiang University of Technology, Hangzhou, 310000, China*
[c] *School of Engineering, London South Bank University, London, SE1 0AA, UK*
[d] *Department of Mechanical Engineering, University of Petroleum and Energy Studies, Dehradun, 248007, India*

ARTICLE INFO

Article history:
Received 16 May 2023
Accepted 14 July 2023
Available online 20 July 2023

Keywords:
Tungsten carbide-cobalt alloy
Chemistry enhanced shear thickening polishing
Fenton's reagent
Material removal mechanism

ABSTRACT

The use of cemented carbides is ubiquitous in many fields especially for mechanical toolings, dies, and mining equipment. Surface finishing of cemented carbide down to atomic level has been a long-standing quest in manufacturing and materials community. For application of complex-shaped cemented carbide components, this work proposes a novel 'chemistry enhanced shear thickening polishing' (C-STP) process using Fenton's reagent to obtain sub 10 nm finished polishing at a rate twice that of the conventional STP. This work offers quantitative insights into the influence of the concentration of Fenton's reagent on the polishing performance. While the material removal rate was seen to be sensitive to the concentration, the surface roughness (Sa) was found to be insensitive to the concentration of Fenton's reagent. The electrochemical experiments proved that Fenton's reagent could effectively reduce the corrosion resistance of tungsten carbide-cobalt alloy. The characterization of polished carbides using XPS and EDS revealed that the cobalt binder gets removed preferentially during C-STP, which explains why the material removal rate during this technique becomes twice that of conventional STP. This study provides a promising method for high efficiency polishing of tungsten carbide-cobalt alloy parts with complex-shaped such as micro-drill.

1. Introduction

Cemented carbides possess excellent mechanical properties such as high strength, wear resistance, nanoindentation hardness and impact resistance. Carbides are widely used as materials for cutting tools [1], molds [2], mining equipment [3] and various other engineering components. Reducing the surface roughness of carbide components can improve their life and their performance [4,5]. Surface roughness directly

* Corresponding author. College of Mechanical Engineering, Zhejiang University of Technology, Hangzhou, 310000, China.
E-mail address: icewater7812@126.com (B. Lyu).

https://doi.org/10.1016/j.jmrt.2023.07.112

influences the optical performance of an optical lens which explains why surface finish of a carbide mold becomes so important in industries to gain competitive edge [6]. The preparation of cutting tool radius and rake face is necessary to eliminate microscopic defects, and improve the surface state for reduced stiction with chips to extend the tool life [7]. Proper treatment of tool surface can facilitate smooth chip flow which improves its wear resistance [8]. Currently, the main precision manufacturing method used for finishing cemented carbide is grinding [9,10]. However, high hardness and low thermal conductivity of carbide leads to the generation of grinding induced defects such as grinding burns or cracks which can compromise tool life [11,12].

Polishing is an effective method to reduce the surface roughness of components [13,14]. Thiyagu et al. [15] adopted magnetorheological fluids to polish the carbide blade which leads to reduced wear losses. Okada et al. [16] found that the surface of cemented carbide became smoother after electron beam irradiation polishing. In addition, Co used as a binder is slightly condensed on the surface, leading to the improvement of water repellency. Beaucamp et al. [17] studied the surface integrity of tungsten carbide with water jet polishing. They found that using a large abrasive grit size with low fluid pressure is preferable to achieve good quality of surface texture. Deng et al. [18] used electrochemical polishing on cemented carbide and obtained a surface roughness (Ra) of 17.6 nm.

Hu et al. [19] performed chemical-mechanical-polishing (CMP) of the YG 8 carbide tool with polishing slurry containing H_2O_2 and the surface roughness (Ra) of the front tool face in the range of 14.4 nm was reported. Mao et al. [20] characterized the chemical principle of tungsten carbide-cobalt alloy in CMP slurry by SEM/EDS, XRD and XPS and found that the chemical action in H_2O_2 is galvanic corrosion. Qin et al. [21] analyzed the elastic–plastic deformation of abrasive in CMP process of cemented carbide and established MRR model considering the synthesized effects of multi-factors, the predicted MRR value and the experimental value is lower than 2.18%.

Usually, the afore-mentioned polishing trials have largely been demonstrated through small scale R&D laboratory based research efforts, whereas, in reality, tools with complex shapes are commercially finished by the use of methods such as drag finishing [22] and abrasive brushing [23]. In a series of efforts, Lyu et al. [24] investigated shear thickening polishing (STP) of carbide tools and reported a surface roughness (Ra) of less than 10 nm at the cutting-edge. This was found to greatly enhance the edge integrity after STP. Span et al. [25] proposed a novel finish machining process in which the medium was made up of non-Newtonian fluid to become compliant with the workpiece at sharp edges. This method could well be applied to surface finish complex shapes as well as for the edge preparation of cutting tools such as drills and end mills. Shao et al. [26,27] utilized fiber-assisted STP method to prepare carbide insert edges. It showed that the polishing angle significantly affected the edge radius and a surface roughness of the order of 5.2 nm was achieved.

STP method [28] utilizes shear thickening effect of the non-Newtonian fluid, which is an efficient and flexible material removal process. STP can be adapted to edge preparation with complex shapes which can meet the requirements of surface quality and integrity at a large scale. While the original STP method was motivated by enhancing the mechanical action of abrasive, the polishing efficiency of materials such as cemented carbide continues to remain much lower due to high wear resistance and hardness of carbides.

Addressing this major impediment, this work proposes a novel chemistry enhanced shear thickening polishing (C-STP) method. The combined merits of chemically active and mechanically abrasive action of polishing slurry were exploited to promote shear thickening effects which has shown promise over conventional STP. This paper elucidates the role and significance of the concentration of the Fenton's reagent in influencing the material removal rate (MRR) and surface roughness of tungsten carbide-cobalt alloy as a testbed study. The chemically corrosive action of Fenton's reagent to the tungsten carbide-cobalt alloy was investigated through the electrochemical analysis as well as additional analysis was performed to study the microstructural changes using techniques such as the SEM, EDS and XPS analysis.

2. Principle of C-STP with Fenton's reagent

Fig. 1 shows a schematic illustration of the C-STP process where the chemical reagent in the polishing slurry due to its high chemical affinity diffuses into the workpiece's surface and reacts with the workpiece (tungsten carbide-cobalt alloy). The surface material of the workpiece oxidizes to a reaction layer which gets easily removed through the simultaneous mechanical action of the grits.

Shear action occurs due to the relative motion between the slurry and the workpiece and the viscosity of the polishing slurry increases rapidly at the contact area. When the shearing velocity reaches a certain value, the shear thickening phenomenon occurs. The solid phase particles in the contact area form a 'particle cluster' wrapped around by the abrasive particles. The solid phase particles improve the ability to hold the abrasives, and the slurry shows solid characteristics in this area. In the process, the chemical reaction layer gets removed by the micro-cutting action of the abrasive. The fresh material of the workpiece becomes exposed again, and the chemical reagent continues to react. The cycle repeats and the combined chemical and mechanical action result in high efficiency and high quality polishing of difficult-to-cut materials such as cemented carbides [29,30].

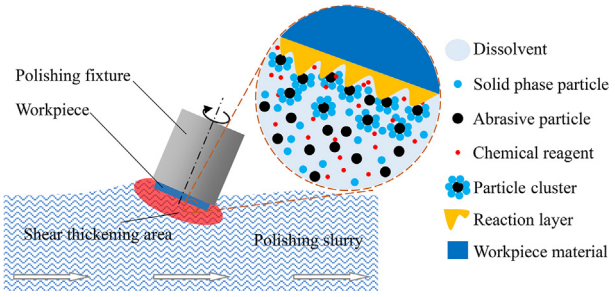

Fig. 1 – Schematic of C-STP process.

Fenton's reaction was first proposed by the French scientist Fenton, the reagent composed of Fe^{2+} and H_2O_2 is referred to as Fenton's reagent [31,32]. Fenton's reaction is a complex process and a common view that describes the process is based on the free radical theory proposed by Harber and Weiss, in which the main reactions formula are [33]:

$$Fe^{2+} + H_2O_2 \rightarrow \cdot OH + OH^- + Fe^{3+} \quad (1)$$

$$Fe^{3+} + H_2O_2 \rightarrow Fe^{2+} + \cdot OH + H^+ \quad (2)$$

H_2O_2 can generate hydroxyl radicals (·OH) catalyzed by Fe^{2+}. The strong oxidizing ability of Fenton's reagent is mainly attributed to ·OH. Its oxidation electrode potential can reach up to 2.8 V [34] as shown in Table 1, which is lower than F_2 but far higher than H_2O_2.

There are many other factors that can affect Fenton's reaction rate, such as reaction time, input of Fe^{2+}, input of H_2O_2, initial pH of the solution and reaction temperature [35]. The oxidation capacity of Fenton's reagent becomes stronger with the increase of Fe^{2+} and H_2O_2 in a certain range and there is an optimal ratio of Fe^{2+} and H_2O_2 so that the mechanical removal rate of shear thickening could match the chemical corrosion rate of Fenton's reagent. The key to achieving the high efficiency polishing target relies on this ratio which was the core mission in undertaking this investigation.

3. Experiment setup

3.1. Pretreatment of tungsten carbide-cobalt alloy samples

The workpiece used for the polishing experiments was cemented carbide, YG-8 supplied by Chengdu Tool research institute Co., LTD, China. The material composition included WC grains with Cobalt (Co) binder wherein Co accounts for about 8 wt.%. To facilitate the characterization of polishing performance samples with a square shape with a size of 13 × 13 × 5 mm were selected for the polishing experiments. The mechanical properties of YG-8 are shown in Table 2. It can be seen that the carbide sample has high hardness and flexural strength. The samples were initially hand polished with the 800# diamond sandpaper such that the initial surface roughness Sa of 120 ± 10 nm was used at the start of the experiments.

3.2. Preparation of C-STP slurry

The C-STP slurry with Fenton's reagent was prepared containing polyhydroxy polymers, abrasive particles, H_2O_2, $FeSO_4$ and deionized water. H_2O_2 and $FeSO_4$ were added into deionized water and stirred well obtained Fenton's solution. Then 8000# diamond abrasive particles and solid phase polyhydroxy polymers with an average particle size of 11.0 μm were added into deionized water and stirred well obtained Non-Newtonian fluid. Finally, mixed the Fenton's solution and Non-Newtonian fluid, the mixture was thoroughly stirred to obtain a C-STP slurry with Fenton's reagent.

Table 1 – Potential table of common oxidants.

Oxidant	F_2	OH	O_3	H_2O_2	Cl_2
E^0 (V)	2.87	2.80	2.07	1.78	1.36

Table 2 – Mechanical properties of the polished tungsten carbide-cobalt alloy sample.

Density (g/cm^3)	Hardness (Hv)			Flexural strength (MPa)	Fracture toughness ($MPa \cdot m^{1/2}$)
	100 gf	500 gf	1000 gf		
13.8	1748.99	1634.97	1518.96	1900	9.6

The rheological curve of C-STP slurry with Fenton's reagent is shown in Fig. 2. There are three distinct rheological regions [36], the shear thinning zone at low shear rate, the shear thickening zone at medium shear rate and the shear thinning zone at high shear rate. Maintaining the shear velocity of polishing slurry with the workpiece near the peak in region II produces the polishing slurry with the high apparent viscosity of the order of 100 Pa·s. It can form a 'solid-like flexible abrasive tool' and move around the workpiece to efficiently remove the material from the workpiece surface.

3.3. C-STP experiments

The polishing apparatus used in this work is shown in Fig. 3. The sample of tungsten carbide-cobalt alloy was clamped on the polishing fixture and immersed into the C-STP slurry. The polishing slurry was fed from the polishing tank while the sample and the tool spins. The detailed experimental conditions are shown in Table 3.

A precision electronic analytical balance (ME225S, Sartorius, Germany) with minimum accuracy of 0.01 mg was adopted to estimate the amount of material (weight) removed during polishing and an average of three polishing experiments were considered to obtain the material removal rate (MRR) during the C-STP process. It is usual during polishing to obtain the MRR in length/time unit since the area of polishing remains fixed during the process. In eq (3), ρ is the density of tungsten carbide-cobalt alloy, S is the polishing area and t is the polishing time:

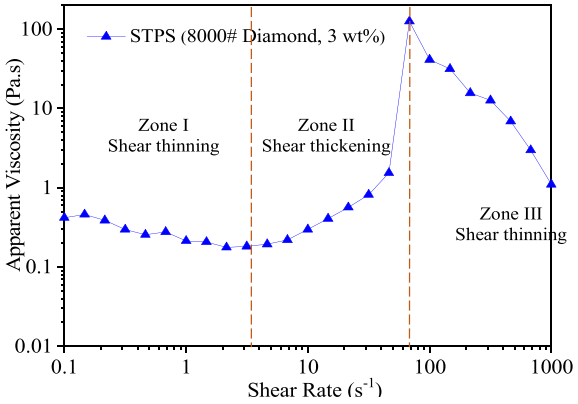

Fig. 2 – The rheological curve of polishing slurry.

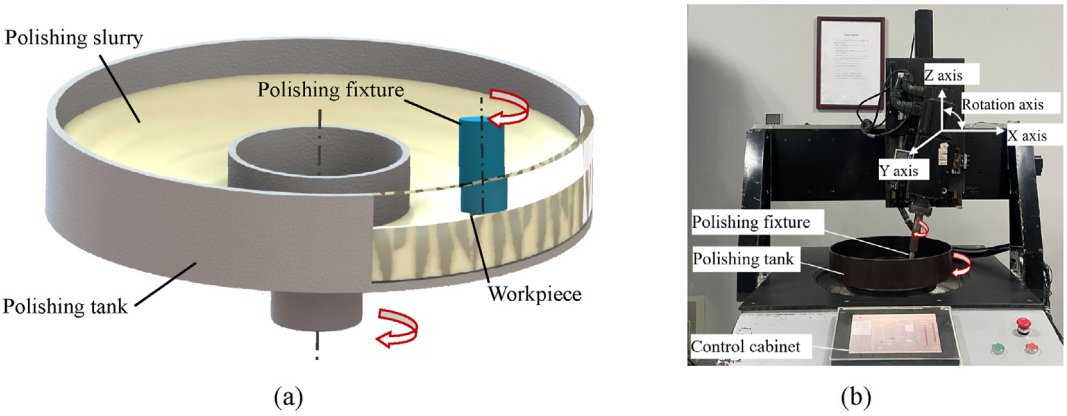

Fig. 3 – Polishing apparatus (a) Schematic illustration of the polishing device (b) Image of the polishing device.

$$MRR = \frac{\Delta m}{\rho \times S \times t} \quad (3)$$

After polishing, the surface topography of the tungsten carbide-cobalt alloy was measured through an optical 3D surface profiler (SuperView W1, Chotest, China). Four points were randomly selected on the sample surface using a 10 × interference objective with a measurement area of 489.5×489.5 μm to obtain the surface roughness (Sa).

The corrosion resistance of tungsten carbide-cobalt alloy samples in different Fenton solutions was tested by an electrochemical workstation (760e, CH Instruments, China). A three-electrode electrolytic cell equipped with a platinum counter electrode of size 20×20×0.2 mm was used. The reference electrode was an Ag/AgCl electrode with saturated KCl solution, and the working electrode was tungsten carbide-cobalt alloy whose working area was 1 cm^2. The open circuit potential (OCP) test was performed before bringing the working electrode to a stable state after the OCP changed to less than 5 mV within 3 min. Taking that OCP as the reference value, the impedance spectrum was measured by applying a sinusoidal disturbance of ±5 mV in the frequency range of 10^{-1} Hz–10^5 Hz. Finally, the dynamic potential polarization curve was tested with the scan rate of 5 mV/s and scan voltage range of −1.1 to 1.1 V (versus to reference electrode).

To check on the elemental composition of the tungsten carbide-cobalt alloy surface, the sample was first cleaned with deionized water after polishing and dried. The samples structure were observed by Scanning Electron Microscope (SIGAM HV, Carl Zeiss, Germany), and the elemental distribution was examined through the Energy Dispersive Spectroscopy (Nano Xflash detector, Bruker, Germany). The atomic valence information of the sample surface was measured by X-ray photoelectron spectroscopy (ESCALAB 250Xi, Thermo, America). Finally, CasaXPS software was used to analyze and process spectral data of W(4f), O(1s), Co(2p), C(1s) and all peaks were corrected with C(1s) 284.8 eV.

Table 3 – Experimental conditions.

Processing conditions	Parameters
Size of the workpiece	13 × 13 × 5 mm
Initial surface roughness (Sa)	120 ± 10 nm
Abrasive	Diamond
Abrasive size	8000#
Abrasive concentration	3 wt.%
Polishing speed	2 m/s
Workpiece rotation speed	10 rpm
Inclination angle	15°
Fenton's reagent	Trial I: 0.10 wt.% H_2O_2 with 0 −1.0 wt.% $FeSO_4$ Trial II: 0.25 wt.% H_2O_2 with 0 −0.8 wt.% $FeSO_4$ Trial III: 0.50 wt.% H_2O_2 with 0 −0.6 wt.% $FeSO_4$
Polishing time per trial	15 min

4. Results and discussions

4.1. *Effect of Fenton's reagent on the polishing performance of tungsten carbide-cobalt alloy*

To study the effect of Fenton's reagent on the polishing performance of tungsten carbide-cobalt alloy, different concentrations of $FeSO_4$ were added into the slurry with 0.1 wt.%, 0.25 wt.% and 0.5 wt.% concentration of H_2O_2 respectively. The influence of the concentration of $FeSO_4$ and H_2O_2 on the MRR and Sa is shown in Fig. 4 and Fig. 5. While using 0.1 wt.% H_2O_2, the peak MRR of about 871.9 nm/min during C-STP of tungsten carbide-cobalt alloy was observed when the concentration of $FeSO_4$ was 0.6 wt.%. However, when a higher concentration of H_2O_2 (0.25 wt.%) was used, the highest MRR of 865.9 nm/min was obtained when the concentration of $FeSO_4$ was 0.5 wt.%. Also, when the concentration of H_2O_2 was further increased to 0.5 wt.%, the highest MRR of 869.9 nm/min was obtained when the concentration of $FeSO_4$ was 0.3 wt.%.

The surface topography maps of the polished tungsten carbide-cobalt alloy samples for various concentrations of $FeSO_4$ and H_2O_2 (wt.%) are shown in Fig. 5. The ratio of Fenton's reagent showed no obvious influence on the surface roughness and Sa of about 7–9 nm was consistently achieved in all cases.

It may be noted that without the addition of $FeSO_4$, MRR showed no significant change when the concentration of H_2O_2

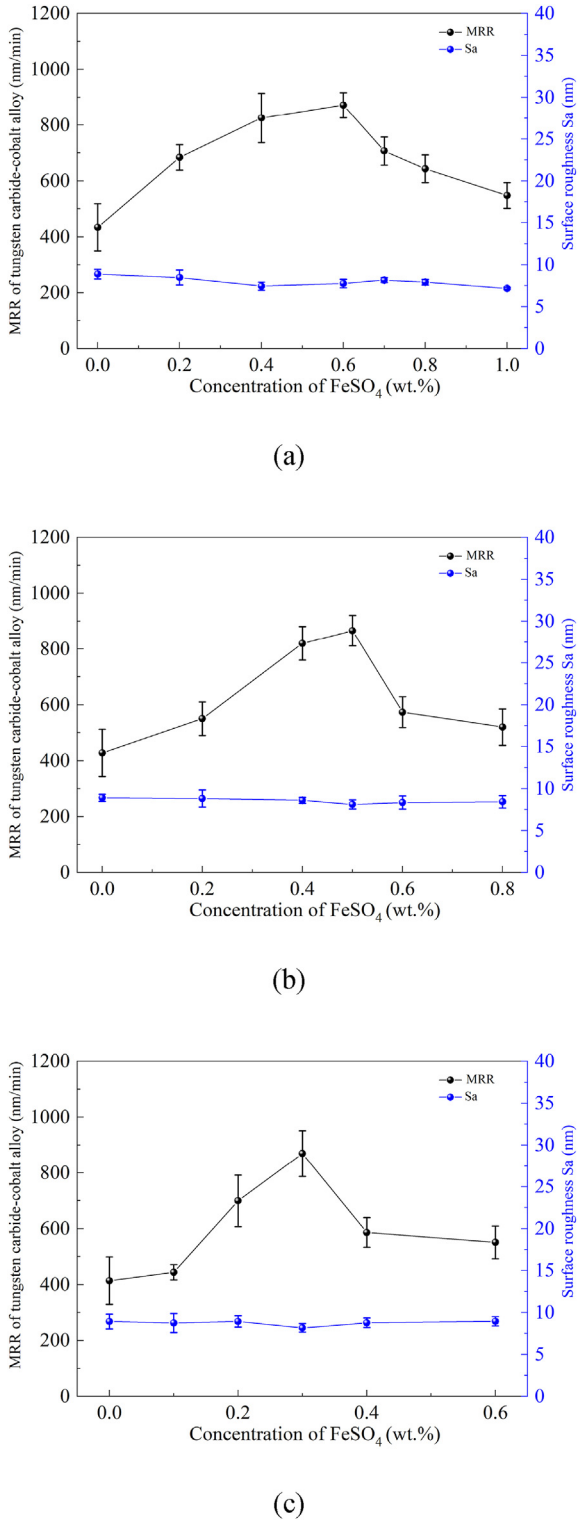

Fig. 4 – Influence of Fenton's reagent with different concentration of $FeSO_4$ at (a) 0.1 wt.% H_2O_2 (b) 0.25 wt.% H_2O_2 and (c) 0.5 wt.% H_2O_2 on the polishing performance of tungsten carbide-cobalt alloy.

was increased from 0.1 wt.% to 0.25 wt.% and 0.5 wt.%. It indicated that the C-STP slurry with H_2O_2 showed no significant chemical reaction with tungsten carbide-cobalt alloy. When the shear thickening effect occurred in the C-STP process, the polishing slurry rapidly transformed from liquid to solid-like state, which hindered the mobility of H_2O_2. Another reason is that, the oxidizing ability of hydrogen peroxide is weaker compared to the Fenton reagents as shown in Table 1.

In summary, Fe^{2+} is essential to form the Fenton reaction for accelerating the MRR during the C-STP process of tungsten carbide-cobalt alloy.

Compared to the C-STP slurry with H_2O_2, the addition of $FeSO_4$ to the slurry with Fenton's reagent enhances the MRR in tungsten carbide-cobalt alloy significantly. The strong oxidizing ability of Fenton's reagent is mainly due to ·OH generated from the Fe^{2+} catalyzing H_2O_2. Its oxidation electrode potential reaches 2.8 V [34], which is higher than H_2O_2. The tungsten carbide-cobalt alloy was oxidized by ·OH and the hard-to-process material was converted into a loose, easily removable layer. Therefore, the mechanical removal efficiency of shear thickening polishing gets greatly improved by oxidation.

The highest MRR of tungsten carbide-cobalt alloy was obtained with the combinations of 0.1 wt.% H_2O_2 + 0.6 wt.% $FeSO_4$, 0.25 wt.% H_2O_2 + 0.5 wt.% $FeSO_4$ and 0.5 wt.% H_2O_2 + 0.3 wt.% $FeSO_4$ and the peak MRR at different concentration of H_2O_2 remained around 868 nm/min. This result indicated that the concentration of $FeSO_4$ required to obtain the highest MRR decreases with the increase of H_2O_2.

What's more, the polishing efficiency decreases with continual increase in the concentration of $FeSO_4$ beyond a certain threshold. Due to the Fenton's reaction, Fe^{2+} does excitation and transmission, so that the chain reaction can continue until entire H_2O_2 gets consumed. If the concentration of $FeSO_4$ is too high, it leads to fast consumption of H_2O_2 which leads to a decrease of MRR. It could also be that the Fenton's reaction produces an excess of ·OH, forming a passivation film on the tungsten carbide-cobalt alloy's surface and preventing the chemical reaction. Thus, the MRR showed a reduction. We shall expand on this aspect in a further study.

4.2. *Electrochemical testing results*

To understand the reaction mechanism of Fenton's reagent and the cause of MRR changes, the corrosion analysis of tungsten carbide-cobalt alloy was performed. The influence of $FeSO_4$ on the MRR showed similarity at different concentrations of H_2O_2, therefore, slurry with 0.1 wt.% H_2O_2 was selected to investigate the influence of different $FeSO_4$ concentrations on the corrosion performance of tungsten carbide-cobalt alloy. The electrochemical test solution consisted of 0.25 mM Na_2SO_4, deionized water and 0.1 wt.% H_2O_2 and different concentration of $FeSO_4$ (0.3 wt.%, 0.6 wt.%, 1.0 wt.%). The corresponding potentiodynamic polarization curves for different concentrations of $FeSO_4$ are shown in Fig. 6(a). The corresponding corrosion potential (E_{coor}) and corrosion current density (I_{coor}) were obtained according to Tafel analysis and the results are shown in Fig. 6(b) and Table 4. As the concentration of $FeSO_4$ increases from 0 to 0.3 wt.%, the corrosion potential decreases rapidly from −0.14 V to −0.34 V. This can be mainly attributed to the ·OH generated by the Fenton's reaction having high oxidizing capacity which effectively reduces the corrosion difficulty of tungsten

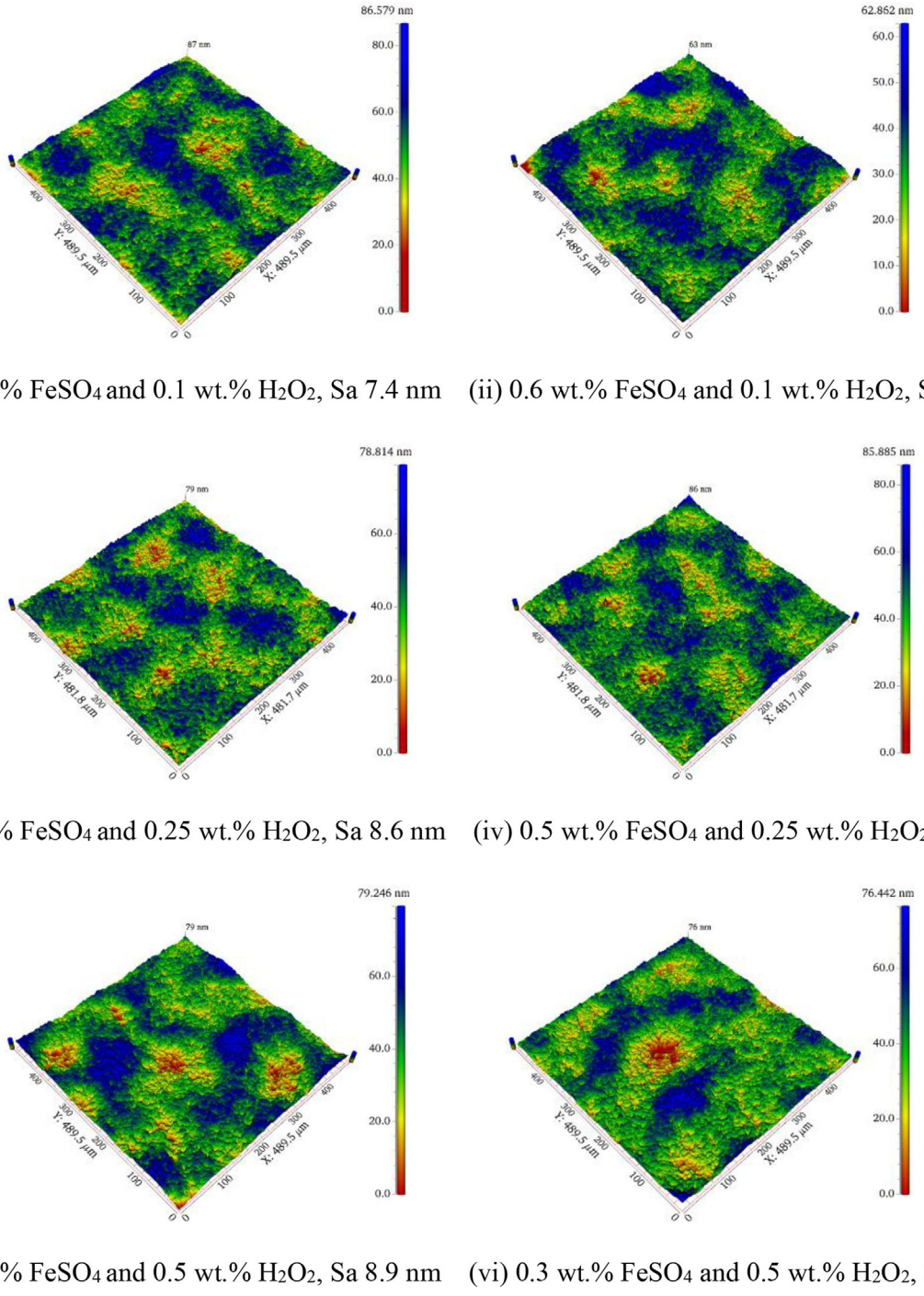

(i) 0.4 wt.% $FeSO_4$ and 0.1 wt.% H_2O_2, Sa 7.4 nm (ii) 0.6 wt.% $FeSO_4$ and 0.1 wt.% H_2O_2, Sa 7.7 nm

(iii) 0.4 wt.% $FeSO_4$ and 0.25 wt.% H_2O_2, Sa 8.6 nm (iv) 0.5 wt.% $FeSO_4$ and 0.25 wt.% H_2O_2, Sa 8.1 nm

(v) 0.2 wt.% $FeSO_4$ and 0.5 wt.% H_2O_2, Sa 8.9 nm (vi) 0.3 wt.% $FeSO_4$ and 0.5 wt.% H_2O_2, Sa 8.2 nm

Fig. 5 – Surface topography of polished tungsten carbide-cobalt alloy samples with different concentrations of $FeSO_4$ and H_2O_2.

carbide-cobalt alloy. As the concentration of $FeSO_4$ increases from 0.3 wt.% to 1.0 wt.%, the corrosion potential remains unchanged. It proved that even excessive ·OH in the polishing slurry would not form a passivation film and impede the chemical reaction.

As the concentration of $FeSO_4$ increases from 0 to 0.6 wt.%, the corrosion current density increases linearly from 45 μA to 158 μA. This result indicates that the generation rate of ·OH increases linearly with the increase of $FeSO_4$ concentration until it reaches 0.6 wt.%, and the corrosion current density also increases linearly. It was a great agreement with the polishing results, where MRR of tungsten carbide-cobalt alloy increases rapidly with increasing of $FeSO_4$ until it reaches a peak value at 0.6 wt.%. At this stage, the increasing ·OH improves the MRR. When the concentration of $FeSO_4$ increases from 0.6 wt.% to 1.0 wt.%, the corrosion current density only increases from 158 μA to 168 μA. It means that excess ·OH does not increase the corrosion rate anymore. However, the MRR showed a decreasing trend when the concentration of $FeSO_4$ exceeds 0.6 wt.% during the polishing experiment.

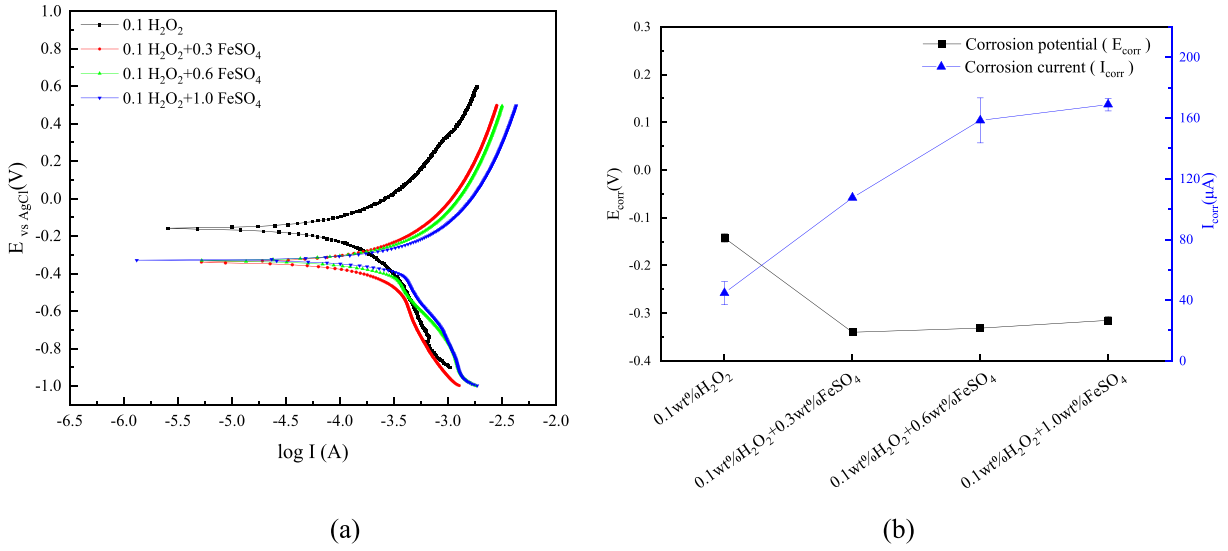

Fig. 6 – (a) Potentiodynamic polarization curves of tungsten carbide-cobalt alloy measured at different concentrations of Fenton's reagent (b) The corrosion current density and the corrosion potential at different concentrations of Fenton's reagent.

The Nyquist curves of the tungsten carbide-cobalt alloy at different $FeSO_4$ concentrations were tested by Electrochemical Impedance Spectroscopy (EIS), and the results are shown in Fig. 7(a). When only H_2O_2 is added to the solution, the curve has only one capacitive resistance arc, and its corresponding equivalent circuit is shown in Fig. 7(b).

When different concentrations of $FeSO_4$ are added to H_2O_2, the number of time constants increases from one to two and the curve has an inductive reactance arc in the low frequency range and a capacitive arc in the high frequency range. The corresponding equivalent circuit is shown in Fig. 7(c). The time constants in the high frequency region are related to electric double layer capacitance on the surface of tungsten carbide-cobalt alloy. This capacitive arc mainly reflects the charging and discharging process of the equivalent circuit, which consists of a charge transfer resistor and an electric double layer capacitor in parallel [37,38]. The inductive reactance arc is mainly caused by the dissolution of the material [39,40].

The overall fitting quality of equivalent circuit can be evaluated by the chi-squared (χ^2) values, and the results is 10.509×10^{-5} for 0.1 wt.% H_2O_2, 9.877×10^{-5} for 0.1 wt.% H_2O_2+0.3 wt.% $FeSO_4$, 9.078×10^{-5} for 0.1 wt.% H_2O_2+0.6 wt.% $FeSO_4$, and 7.879×10^{-5} for 0.1 wt.% H_2O_2+1.0 wt.% $FeSO_4$, respectively. The order of χ^2 is 10^{-5} which means in good fitting quality. The values of the corresponding measurements in the equivalent circuit are shown in Table 5. In the equivalent circuit, the R_{sol} represents the solution resistance. As the electrolyte in the solution is increased, the R_{sol} decreases with the increase of $FeSO_4$. The R_{ct} represents the charge transfer resistance. The *CPE* represents the capacitance associated with the bilayer. As we can see with the addition of $FeSO_4$, the *CPE*-Y_0 increases form rapidly from 376 to 1121 $\mu S\cdot s^n\cdot cm^{-2}$, this results show that the reaction layer on the top surface of tungsten carbide-cobalt alloy changes from dense to loose, and corrosion is promoted by Fenton's reagent with the increase of $FeSO_4$ [41,42]. Meanwhile, the value of *CPE*-n deviates further from 1, which indicates that the surface becomes rougher caused by corrosion [43]. The $R_{s\text{-}f}$ represents the resistance caused by ·OH. The L represents the inductance due to the adsorption and desorption processes of ·OH.

Table 4 – I_{coor} and E_{coor} with different concentrations of Fenton's reagent.

Solution	I_{coor} ($\mu A/cm^{-2}$)	E_{coor} vs. E_{AgCl} (V)
0.1 wt.% H_2O_2	45	−0.14
0.1 wt.% H_2O_2, 0.3 wt.% $FeSO_4$	107	−0.34
0.1 wt.% H_2O_2, 0.6 wt.% $FeSO_4$	158	−0.33
0.1 wt.% H_2O_2, 1.0 wt.% $FeSO_4$	169	−0.31

The polarization resistance R_p had been applied to evaluate the corrosion resistance properties of the material. The Faraday resistance of this electrode system was calculated when the frequency was 0, thus the R_p of the solution system containing H_2O_2 only was just R_{ct}. The R_p of the solution system containing Fenton's reagent was calculated as [40].

$$R_p = \frac{R_{ct}R_{s-f}}{R_{ct+}R_{s-f}} \quad (4)$$

As shown in Table 6, with the increase of $FeSO_4$, the polarization resistance R_p decreases from 258 $\Omega\cdot cm^{-2}$ to 44 $\Omega\cdot cm^{-2}$. After the $FeSO_4$ concentration reaches 0.6 wt.%, the R_p basically stops decreasing. It indicated that the corrosion difficulty does not decrease any further with the increase of the $FeSO_4$ concentration. What's more, the MRR also reaches the maximum value at 0.1 wt.% H_2O_2 with 0.6 wt.% $FeSO_4$.

4.3. *X-ray photoelectron spectroscopy experiment*

To check the Fenton's reaction products with tungsten carbide-cobalt alloy, the samples were soaked in different polishing slurry for 30 min. The surface composition was

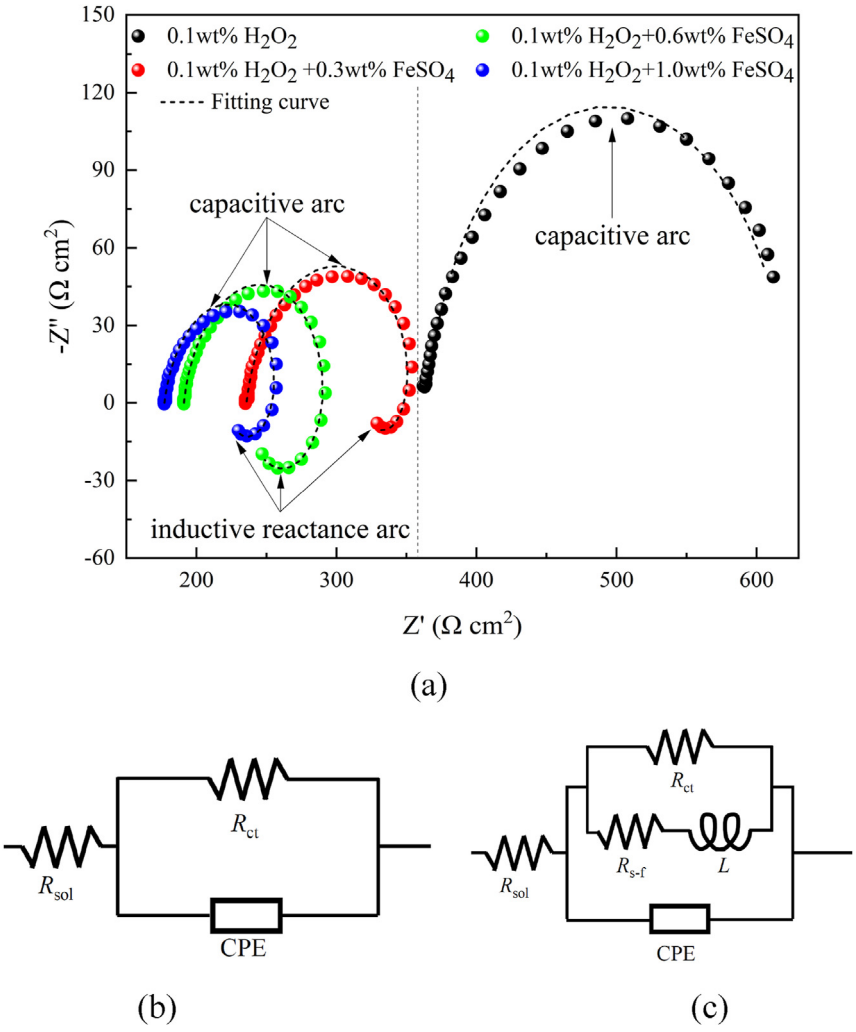

Fig. 7 – (a) Nyquist diagram obtained from EIS of different Fenton's reagents (b) The equivalent circuit derived from the EIS results (c) The equivalent circuit derived from the EIS results.

analyzed by X-ray Photoelectron Spectroscopy (XPS), and the W, O and Co spectra are shown in Fig. 8.

As shown in Fig. 8(a), the deconvolution of the W(4f) spectra reveals three peaks [44]: the Red dashed line is related to WC with the binding energy of 31.8 eV, as well as the green dashed line is related to WO_2 with the binding energy of 32.2 eV, and the blue dashed line is related to WO_3 with the binding energy of 35.5 eV.

Compared to the original STP slurry, the spectra area of WO_3 (blue dashed line) soaked in C-STP slurry was significantly larger, which indicated that the strong oxidation reaction leads to a large amount of WC transforming into WO_3. The samples soaked in STP slurry only have a small amount of WO_2 and WO_3 on the surface, which may be caused by slight oxidation of WC that occurred with oxygen in slurry or air.

As shown in Fig. 8(b), the deconvolution of O(1s) spectra reveals two peaks [45]: the cyan dashed line is related to OH^- with the binding energy of 532.7 eV, and the magenta dashed line is related to tungsten oxide with the binding energy of 530.8 eV. The magenta area of C-STP slurry was larger than that of STP slurry, which indicated the production of WO_3.

As shown in Fig. 8(c), the deconvolution of the Co(2p) spectra revealed two peaks: the dark yellow dashed line is related to Co with the binding energy of 782 eV, and the navy blue dashed line is related to Co^{2+} with the binding energy of 787 eV [44]. The samples soaked in C-STP slurry only existed one characteristic spectrum, which is directive to $Co(OH)_2$. Therefore, it is certain that the strong oxidation of ·OH completely transforms Co to $Co(OH)_2$.

Based on the analysis of the XPS spectra, it can be inferred that the WC and Co were oxidized by ·OH, through the chemical reactions [46,47]:

$$WC + \cdot OH \rightarrow WO_3 + CO_2 \uparrow + H_2O \quad (5)$$

$$Co + \cdot OH \rightarrow Co(OH)_2 + H_2O \quad (6)$$

4.4. *Energy Dispersive Spectroscopy (EDS)*

The samples of tungsten carbide-cobalt alloy were polished with the original STP slurry (without Fenton's reagent) and C-STP slurry with Fenton's reagent (0.1 wt.% H_2O_2 and 0.6 wt.% $FeSO_4$), and the concentrations of elements were investigated

Table 5 – The EIS of tungsten carbide-cobalt alloy at different Fenton's reagents and the proposed equivalent circuit.

Solution	R_{sol} ($\Omega\cdot cm^{-2}$)	R_{ct} ($\Omega\cdot cm^{-2}$)	CPE-Y_0 ($\mu S\cdot s^n\cdot cm^{-2}$)	CPE-n	R_{s-f} ($\Omega\cdot cm^{-2}$)	L ($H\cdot cm^{-2}$)
0.1 wt.% H_2O_2	365	258	376	0.93	/	/
0.1 wt.% H_2O_2, 0.3 wt.% $FeSO_4$	236	242	1121	0.86	133	247
0.1 wt.% H_2O_2, 0.6 wt.% $FeSO_4$	191	74	1483	0.87	114	129
0.1 wt.% H_2O_2, 1.0 wt.% $FeSO_4$	177	82	1751	0.85	100	54

Table 6 – The R_p of different concentrations of solution.

Solution	R_p ($\Omega\cdot cm^{-2}$)
0.1 wt.% H_2O_2	258
0.1 wt.% H_2O_2, 0.3 wt.% $FeSO_4$	85
0.1 wt.% H_2O_2, 0.6 wt.% $FeSO_4$	45
0.1 wt.% H_2O_2, 1.0 wt.% $FeSO_4$	44

by the Energy Dispersive Spectroscopy (EDS) after polishing, the elemental composition obtained by semi-quantitative analysis of the energy spectra are shown in Table 7. The contents of four elements W, C, Co and O in the tungsten carbide-cobalt alloy after polishing with original STP slurry were 82.16 wt.%, 8.4 wt.%, 8.17 wt.% and 1.22 wt.%, and the contents of W, C, Co and O polishing with C-STP slurry are 89.69 wt.%, 8.58 wt.%, 0.00 wt.%, 1.73 wt.%. There is a small increase of element O, which indicates that Fenton's reagent has enough oxidizing ability and the oxides are formed on the surface. It should be especially noted that the Co element disappears completely after polishing with C-STP slurry.

The distribution of elements on the surface of tungsten carbide-cobalt alloy after STP process is shown in Fig. 9(a), W (green) and C (blue) are concentrated on the large grains, and Co (rose red) is concentrated in the spaces between the grains. The distribution of elements on the surface of tungsten carbide-cobalt alloy after C-STP process is shown in Fig. 9(b), only W and C are concentrated in the large grains. The Co is randomly distribution on the grains, especially if there is no Co distribution between the grains which is completely different from STP process.

Combined with the EDS surface scan results, as shown the SEM microscopic topography in Fig. 9(c), the tungsten carbide-cobalt alloy polishing with STP slurry consists of WC grains and Co, and the interstices of WC are filled with Co. As shown the SEM microscopic topography in Fig. 9(d), the filler between WC grains after polishing with C-STP slurry obviously disappeared, and lots of small pits were produced which means the strong oxidation of Fenton's reagent corrodes Co and completely removes it.

4.5. *Material removal mechanism of tungsten carbide-cobalt alloy*

Combining the results of EDS and XPS analysis, the material removal mechanism of tungsten carbide-cobalt alloy with Fenton's C-STP slurry is shown in Fig. 10. In the first stage, the Co element on the surface of tungsten carbide-cobalt alloy is firstly oxidized to $Co(OH)_2$ by the strong oxidation of ·OH, because it has a lower reaction potential than WC. Subsequently, some part of WC gets oxidized to WO_3. Additionally, the reaction layer produced on the top surface is loose, which means easier to been removed than the tungsten carbide-cobalt alloy. In the second stage, the shear thickening effect forms a cluster of particles containing abrasive particles, and the $Co(OH)_2$ on the surface layer of tungsten carbide-cobalt alloy gets rapidly removed. In the third stage, the Co element which is used as the binding phase in tungsten carbide-cobalt alloy material gets removed. There are no connections between hard phase WC, so the WC grains and its loose oxides are relatively easy to be removed by the abrasive particles. Finally, the fresh surface is exposed again, which can accelerate the oxidation reaction, both the chemical and

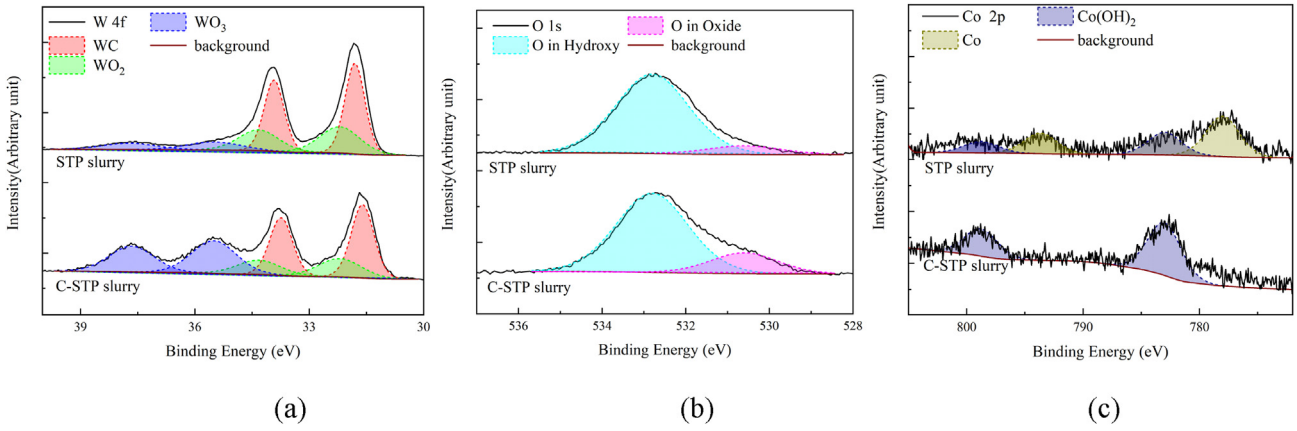

Fig. 8 – XPS spectra of tungsten carbide-cobalt alloy after soaking in different slurry (a) XPS W(4f) spectra (b) XPS O(1S) spectra (c) XPS Co(2p) spectra.

Table 7 – The composite of carbide cemented after polished by different slurry.

Element	W (wt.%)	C (wt.%)	Co (wt.%)	O (wt.%)
STP slurry	82.16	8.44	8.17	1.22
C-STP slurry with Fenton's reagent	89.69	8.58	0.00	1.73

mechanical action synergies improve the polishing efficiency of tungsten carbide-cobalt alloy.

4.6. *Polishing experiments with optimal parameters*

The relationship between surface roughness and polishing duration for the tungsten carbide-cobalt alloy samples polished by C-STP slurry was benchmarked against traditional STP which is shown in Fig. 11. The ratio H_2O_2 and $FeSO_4$ corresponding to the highest MRR were selected for C-STP process (0.1 wt.% H_2O_2 with 0.6 wt.% $FeSO_4$, 0.25 wt.% H_2O_2 with 0.5 wt.% $FeSO_4$ or 0.5 wt.% H_2O_2 with 0.3 wt.% $FeSO_4$). It was found that Fenton's reagent could effectively reduce surface roughness and three different ratio combinations of Fenton's reagent tested during this work showed negligible influence on the decreasing trend of surface roughness.

Therefore, the surface topography of the typical two sets of experiments (original STP slurry and C-STP slurry with 0.1 wt.% H_2O_2, 0.6 wt.% $FeSO_4$) at different times are shown in Fig. 12. Initially, several scratches were seen on the surface of tungsten carbide-cobalt alloy as shown in Fig. 12(a) and (f). As shown in Fig. 12(c), the STP process sample still showed many scratches, and the surface roughness (Sa) was about 35 nm after polishing for 6 min. As shown in Fig. 12(h), C-STP process samples showed only fewer deep pits remaining, and the surface roughness dropped to about 14 nm after 6 min polishing. At the end, the surface

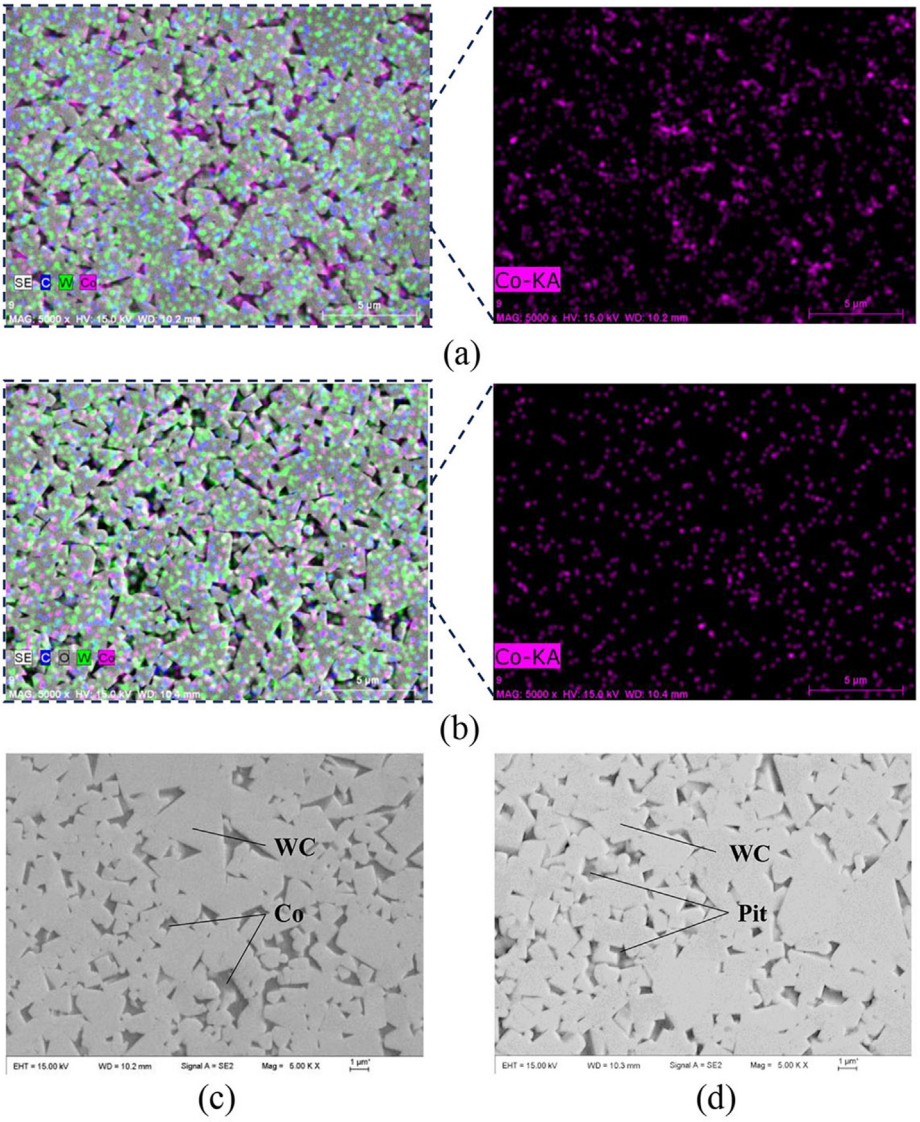

Fig. 9 – Elements distribution of tungsten carbide-cobalt alloy after polishing by different slurry (a) Polishing by STP slurry (b) Polishing by C-STP slurry. And surface topography of tungsten carbide-cobalt alloy after polishing by different slurry (c) Polishing by STP slurry (d) Polishing by the C-STP slurry.

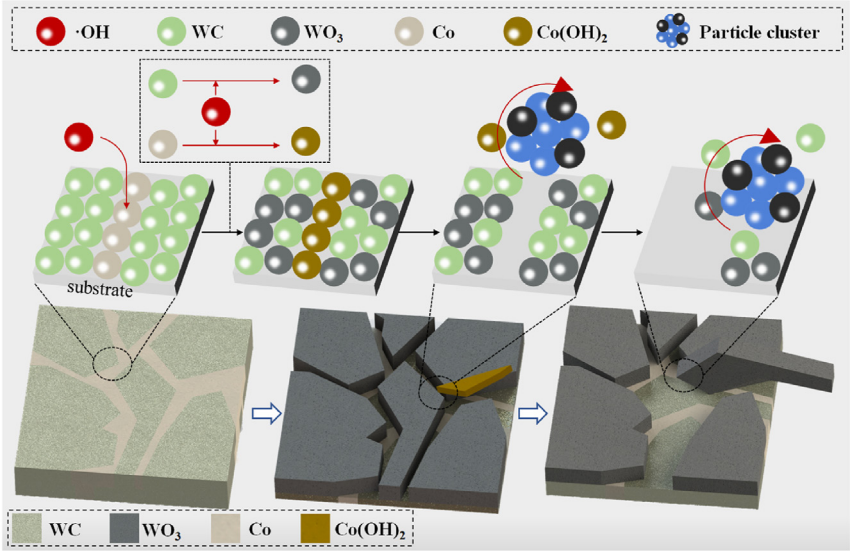

Fig. 10 – Material removal mechanism of tungsten carbide-cobalt alloy by C-STP with Fenton's reagent.

roughness of both tungsten carbide-cobalt alloy samples maintained around 8.5 nm which was shown in Fig. 12(e) and (j). From the final comparison of samples before and after polishing shown in Fig. 11, it can be seen that a mirror finish tungsten carbide-cobalt alloy can be obtained with the C-STP process.

4.7. *Application*

As mentioned in the introduction, cemented carbide is the main materials of cutting tools and the polishing of surface and cutting-edge can improve tool service performance. However, the micro-drill with complex cutting-edge shape is difficult to polish, and the processing efficiency is also very low. The polishing of the micro drill is a problem in the industry.

The micro-drills (Shenzhen Jinzhou Precision Technology Co., China) made of tungsten carbide-cobalt alloy (YG-6) were selected to verify the potential application of C-STP with Fenton's reagent. Fig. 13 (a) illustrates the shape structure of a micro-drill point after grinding, with a diameter of 0.4 mm, which clearly displays numerous defects on the cutting-edge.

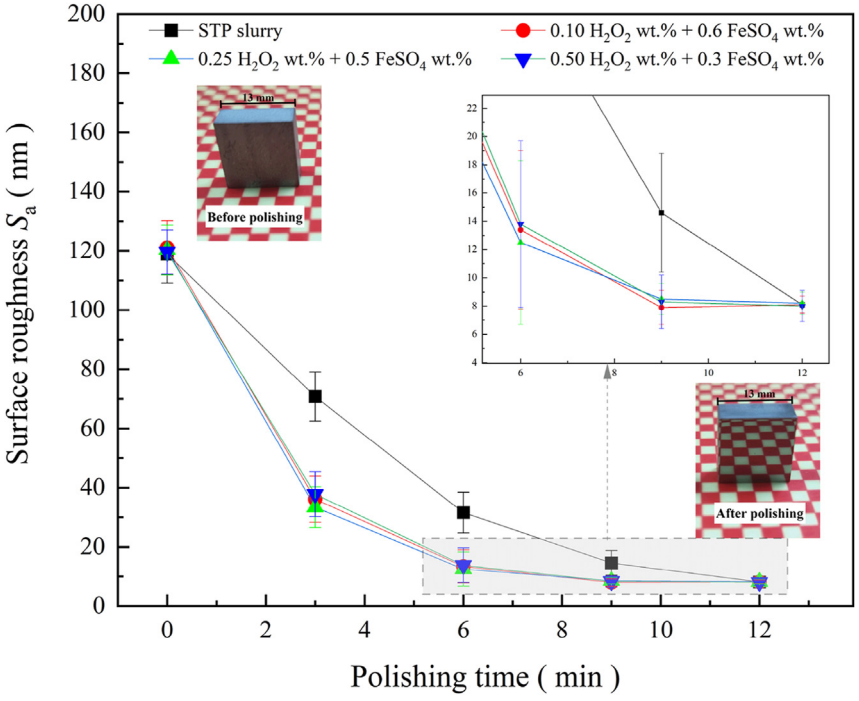

Fig. 11 – The relationship between surface roughness and time of tungsten carbide-cobalt alloy processed by different slurry.

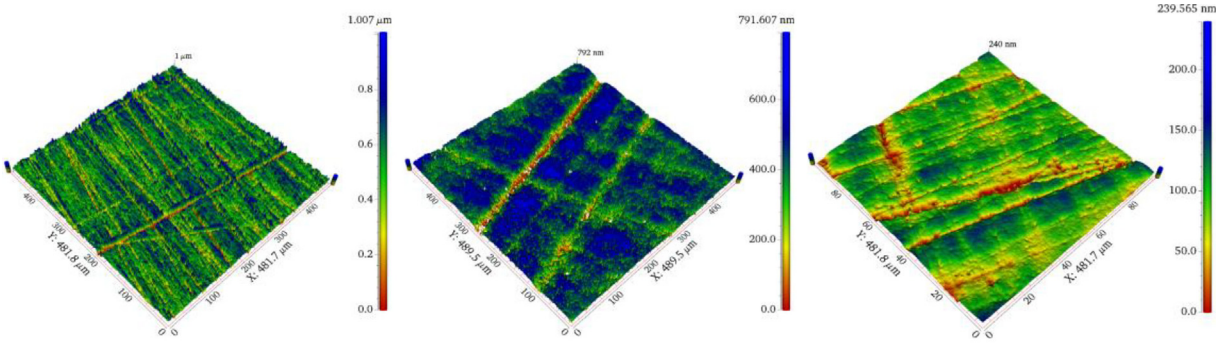

(a) 0 min, Sa 124.2 nm. (b) 3 min, Sa 81.6 nm. (c) 6 min, Sa 29.9 nm.

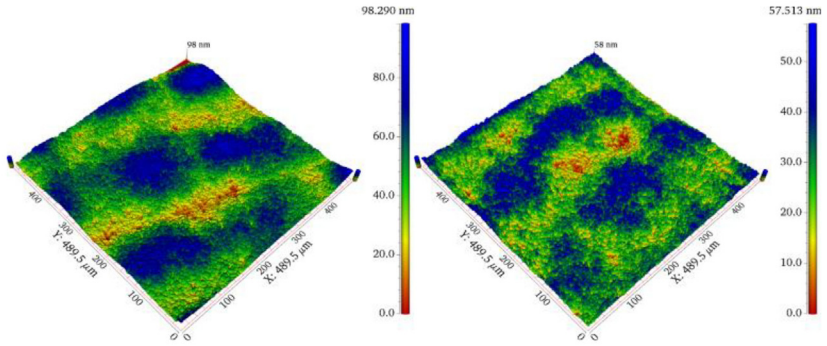

(d) 9 min, Sa 13.0 nm. (e) 12 min, Sa 8.4 nm.

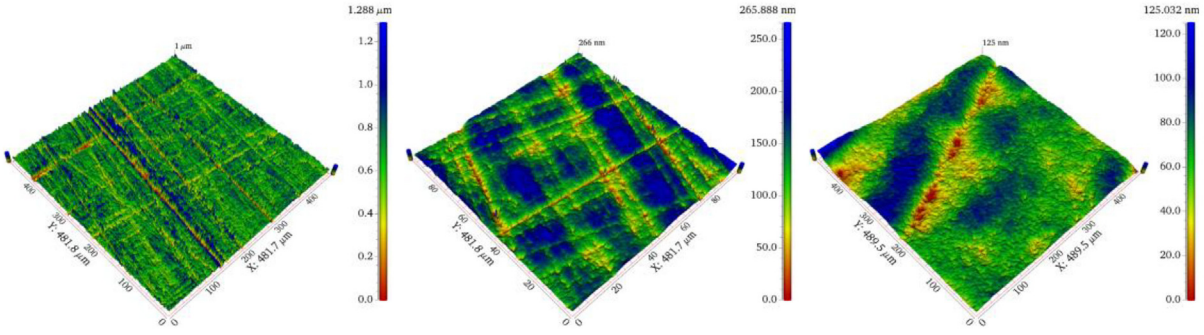

(f) 0 min, Sa 116.3 nm. (g) 3 min, Sa 30.2 nm. (h) 6 min, Sa 14.4 nm.

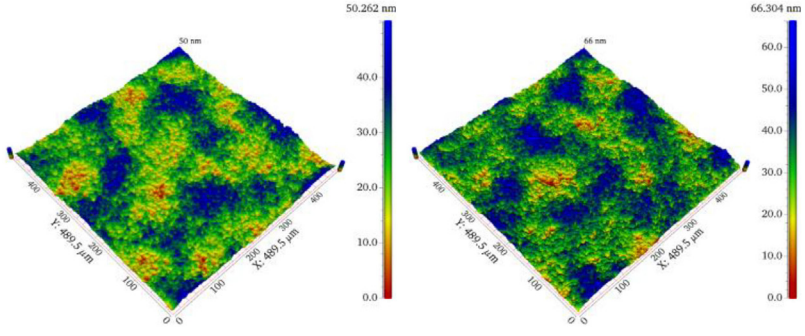

(i) 9 min, Sa 8.7 nm. (j) 12 min, Sa 8.5 nm.

Fig. 12 – Typical surface topography of tungsten carbide-cobalt alloy at different times polishing with different slurry (a)–(e) Polished by STP slurry at different times (f)–(j) Polished by C-STP slurry at different times.

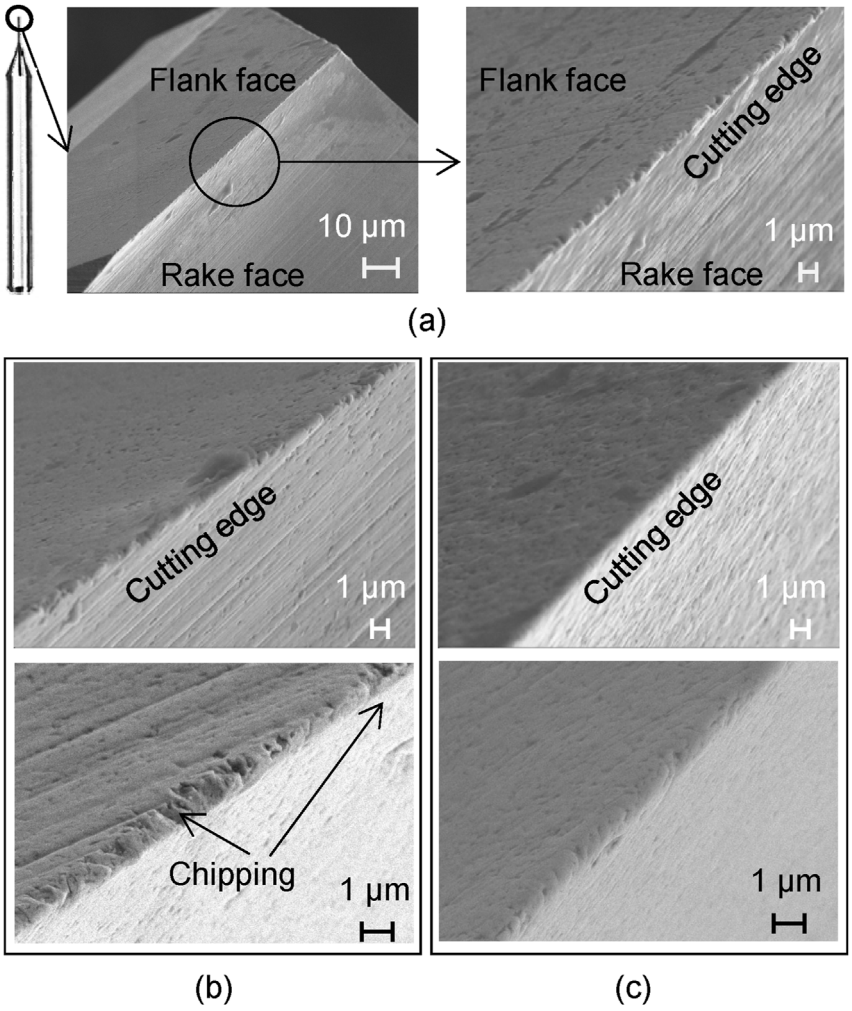

Fig. 13 – Comparison of cutting-edge polishing of micro-drill with different slurry (a) Illustration of cutting-edge without polishing, (b) Polishing by STP slurry, (c) Polishing by C-STP slurry.

To solve this problem, the STP and C-STP methods were employed to polish the micro-drill for 3 min. As shown in Fig. 13 (b), where there are still some remaining chippings on the cutting-edge and grinding marks on rake face after 3 min of STP. The micro-drill after 3 min of C-STP (using Fenton's reagent: 0.1 wt.% H_2O_2, 0.6 wt.% $FeSO_4$) is shown in Fig. 13 (c), where it is obvious that the cutting-edge is completely smoothed and the grinding marks on the rake face have been eliminated. The elimination of micro defects on cutting-edge expect to improve machining process reliability, reduce wear rates, and improve cutting performance [7,19]. This indicates that Fenton's reagent can effectively improve the MRR of tungsten carbide-cobalt alloy and provide a potential manufacturing technology for the surface process of complex tools.

5. Conclusion

In this paper, for application of complex-shaped tungsten carbide-cobalt alloy components, a novel "chemistry enhanced shear thickening polishing" (C-STP) process using Fenton's reagent to obtain sub 10 nm finished polishing at a rate twice that of the conventional STP was developed. Experimental trials were made to study the influence of different ratio of H_2O_2 and $FeSO_4$ on the polishing performance and to examine the mechanism of material removal mechanism. Based on the afore-mentioned discussions, following broad conclusions were drawn.

(1) For a given concentration of $FeSO_4$, a threshold magnitude of H_2O_2 exists which yields the maximum material removal rate (MRR). In case of tungsten carbide, the newly developed C-STP process resulted in a peak MRR of about 868 nm/min when using 0.1 wt.% H_2O_2 with 0.6 wt.% $FeSO_4$, 0.25 wt.% H_2O_2 with 0.5 wt.% $FeSO_4$, and 0.5 wt.% H_2O_2 with 0.3 wt.% $FeSO_4$. The improvement in the MRR using C-STP process was twice that of the traditional STP process suggesting that the presence of Fenton's reagent greatly improves the polishing efficiency. While C-STP process improved the MRR, its influence on surface roughness was found insignificant. Almost all trials resulted in sub 10 nm roughness.

(2) The electrochemical tests, EDS, XPS results of the polished samples revealed that the ·OH generated by Fenton's reagent can have a strong oxidizing effect, which can effectively reduce the corrosion resistance of cemented carbide. The binding phase, Co gets easily oxidized and removed in a large amount compared to the WC matrix. As the Co gets removed at an accelerated rate during C-STP, it gets easier to remove the resulting oxides at an improved material removal rate during the proposed C-STP process.

(3) The proposed C-STP process helped reduced the surface roughness on cemented carbide from an initial value of Sa 120 ± 10 nm to 8.4 ± 0.5 nm in less than 9 min. This improvement became possible only due to the presence of Fenton's reagent which results in enhancing the shear thickening effect during the polishing process. Besides, it provides an emergent surface process technique for micro-drill with complex shapes, which eliminates the burrs on cutting-edge within 3 min.

Declaration of Competing Interest

The authors declare that they have no known competing financial interests or personal relationships that could have appeared to influence the work reported in this paper.

Acknowledgments

This paper received financial support in form of National Natural Science Foundation of China (52175441), Zhejiang Provincial Natural Science Foundation of China (LD22E050010), National Natural Science Foundation of China (52175442) and a travel scholarship from the China Scholarship Council (No. 202208330333) for secondment of JW at LSBU for working closely with Prof Goel.

SG would like to acknowledge the funding support from UKRI via Grants No. EP/S036180/1and EP/T024607/1, feasibility study awards to LSBU from the UKRI National Interdisciplinary Circular Economy Hub (EP/V029746/1) and Transforming the Foundation Industries: a Network+ (EP/V026402/1).

REFERENCES

[1] García J, Ciprés VC, Blomqvist A, Kaplan B. Cemented carbide microstructures: a review. Int J Refract Metals Hard Mater 2019;80:40–68.

[2] Liang Z, Du Y, Ma Y, Su Z, Chen R, Yuan H, et al. Development of polycrystalline diamond micro end mill for milling-grinding combined machining of cemented carbide. J Manuf Process 2022;79:844–53.

[3] Dewangan S, Chattopadhyaya S. Critical analysis of wear mechanisms in cemented carbide. J Mater Eng Perform 2015;24:2628–36.

[4] Chen H, Xu Q, Wang J, Li P, Yuan J, Lyu B, et al. Effect of surface quality on hydrogen/helium irradiation behavior in tungsten. Nucl Eng Technol 2022;54(6):1947–53.

[5] Chen H, Wang L, Peng F, Xu Q, Xiong Y, Wu Y, et al. Hydrogen retention and affecting factors in rolled tungsten: Thermal desorption spectra and molecular dynamics simulations. Int J Hydrog Energy 2023.

[6] Namba Y, Shimomura T, Fushiki A, Beaucamp A, Inasaki I, Kunieda H, et al. Ultra-precision polishing of electroless nickel molding dies for shorter wavelength applications. CIRP annals 2008;57(1):337–40.

[7] Zhang S, Zou B, Liu Y, Wang Y, Huang C, Liu Z, et al. Edge passivation and quality of carbide cutting inserts treated by wet micro-abrasive blasting. Int J Adv Des Manuf Technol 2018;96(5):2307–18.

[8] Ventura CEH, Köhler J, Denkena B. Cutting-edge preparation of PCBN inserts by means of grinding and its application in hard turning. CIRP Journal of Manufacturing Science and Technology 2013;6(4):246–53.

[9] Zhang Y, Xu X. Influence of surface topography evolution of grinding wheel on the optimal material removal rate in grinding process of cemented carbide. Int J Refract Metals Hard Mater 2019;80:130–43.

[10] Habrat WF. Effect of bond type and process parameters on grinding force components in grinding of cemented carbide. Procedia Eng 2016;149:122–9.

[11] Yang J, Roa JJ, Schwind M, Odén M, Johansson-Jõesaar MP, Llanes L. Grinding-induced metallurgical alterations in the binder phase of WC-Co cemented carbides. Mater Charact 2017;134:302–10.

[12] Gao P, Liang Z, Wang X, Zhou T, Li S, Zhang S, et al. Cutting-edge damage in grinding of cemented carbides micro end mills. Ceram Int 2017;43(14):11331–8.

[13] Luo H, Ajmal KM, Liu W, Yamamura K, Deng H. Polishing and planarisation of single crystal diamonds: state of the art and perspectives. Int J Extrem Manuf 2021;3(2):022003.

[14] Guo J, Shi X, Song C, Niu L, Cui H, Guo X, et al. Theoretical and experimental investigation of chemical mechanical polishing of W–Ni–Fe alloy. Int J Extrem Manuf 2021;3(2):025103.

[15] Thiyagu M, Karunamoorthy L, Arunkumar N. Thermal and tool wear characterisation of graphene oxide coated through magnetorheological fluids on cemented carbide tool inserts. Arch Civ Mech Eng 2019;19(4):1043–55.

[16] Okada A, Kitada R, Okamoto Y, Uno Y. Surface modification of cemented carbide by EB polishing. CIRP Ann Manuf Technol 2011;60(1):575–8.

[17] Beaucamp A, Namba Y, Messelink W, Walker D, Charlton P, Freeman R. Surface integrity of fluid jet polished tungsten carbide. Procedia Cirp 2014;13:377–81.

[18] Deng H, Huang R, Liu K, Zhang X. Abrasive-free polishing of tungsten alloy using electrochemical etching. Electrochem Commun 2017;82:80–4.

[19] Hu Z, Qin C, Chen ZC, Yang Z, Fang T, Mao M. Experimental study of chemical mechanical polishing of the final surfaces of cemented carbide inserts for effective cutting austenitic stainless steel. Int J Adv Manuf Technol 2018;95:4129–40.

[20] Mao M, Chen W, Liu J, Hu Z, Qin C. Chemical mechanism of chemical mechanical polishing of tungsten cobalt cemented carbide inserts. Int J Refract Metals Hard Mater 2020;88:105179.

[21] Qin C, Hu Z, Tang A, Yang Z, Luo S. An efficient material removal rate prediction model for cemented carbide inserts chemical mechanical polishin. Wear 2020;452:203293.

[22] Lv D, Wang Y, Yu X, Chen H, Gao Y. Analysis of abrasives on cutting-edge preparation by drag finishing. Int J Adv Manuf Technol 2022;119(5):3583–94.

[23] Bergs T, Schneider SAM, Amara M, Ganser P. Preparation of symmetrical and asymmetrical cutting-edges on solid cutting tools using brushing tools with filament-integrated diamond grits. Procedia CIRP 2020;93:873–8.

[24] Lyu BH, He QK, Chen SH, Shao Q, Chen Y, Geng ZY. Experimental study on shear thickening polishing of cemented carbide insert with complex shape. Int J Adv Manuf Technol 2019;103(1):585–95.
[25] Span J, Koshy P, Klocke F, Müller S, Coelho R. Dynamic jamming in dense suspensions: surface finishing and edge honing applications. CIRP Ann Manuf Technol 2017;66(1):321–4.
[26] Shao L, Zhou Y, Fang W, Wang J, Wang X, Deng Q, et al. Preparation of cemented carbide insert cutting-edge by flexible fiber-assisted shear thickening polishing method. Micromachines 2022;13(10):1631.
[27] Shao L, Ke M, Wang J, Lyu B, Wang X, Yuan J. Experimental study on flexible fiber assisted stress rheological passivation and polishing of complex edge of cemented carbide insert. Diamond Abrasives Eng 2022;42(1):1–9.
[28] Li M, Lyu B, Yuan J, Dong C, Dai W. Shear-thickening polishing method. Int J Mach Tool Manufact 2015;94:88–99.
[29] Wang J, Lyu B, Jiang L, Shao Q, Deng C, Zhou Y, et al. Chemistry enhanced shear thickening polishing of Ti–6Al–4V. Precis Eng 2021;72:59–68.
[30] Wang J, Zhou Y, Qiao Z, Goel S, Wang J, Wang X, et al. Surface polishing and modification of Ti-6Al-4V alloy by shear thickening polishing. Surf Coat Technol 2023:129771.
[31] Neyens E, Baeyens J. A review of classic Fenton's peroxidation as an advanced oxidation technique. J Hazard Mater 2003;98(1–3):33–50.
[32] Shishkin A, Goel G, Baronins J, Ozolins J, Hoskins C, Goel S. Using circular economy principles to recycle materials in guiding the design of a wet scrubber-reactor for indoor air disinfection from coronavirus and other pathogens. Environ Technol Innovat 2021;22:101429.
[33] Pignatello JJ, Oliveros E, MacKay A. Advanced oxidation processes for organic contaminant destruction based on the Fenton reaction and related chemistry. Crit Rev Environ Sci Technol 2006;36(1):1–84.
[34] Nagarajan S, Skillen NC, Fina F, Zhang G, Randorn C, Lawton LA, et al. Comparative assessment of visible light and UV active photocatalysts by hydroxyl radical quantification. J Photochem Photobiol Chem 2017;334:13–9.
[35] Miller CM, Valentine RL. Hydrogen peroxide decomposition and quinoline degradation in the presence of aquifer material. Water Res 1995;29(10):2353–9.
[36] Galindo-Rosales FJ, Rubio-Hernández FJ, Sevilla A, Ewoldt RH. How Dr. Malcom M. Cross may have tackled the development of "An apparent viscosity function for shear thickening fluids. J Non-Newtonian Fluid Mech 2011;166(23–24):1421–4.
[37] Orazem ME, Tribollet B. Electrochemical impedance spectroscopy. John Wiley & Sons; 2017.
[38] Bard AJ, Inzelt G, Scholz F. Electrochemical dictionary. Berlin, Heidelberg: Springer Berlin Heidelberg; 2012.
[39] Cao C. Principles of electrochemistry of corrosion. 3rd ed. Beijing: Chemical Industry Press; 2008 [in Chinese)].
[40] Liu J, Jiang L, Wu H, Zhong X, Qian L. Performance of carboxyl groups in chemical mechanical polishing of GCr15 bearing steel: effects of carbon chain length and pH. Tribol Lett 2021;69(4):1–11.
[41] Amin MA, Abd El-Rehim SS, El-Sherbini EEF, Bayoumi RS. The inhibition of low carbon steel corrosion in hydrochloric acid solutions by succinic acid: Part I. Weight loss, polarisation, EIS, PZC, EDX and SEM studies. Electrochim Acta 2007;52(11):3588–600.
[42] Liu J, Jiang L, Wu H, Zhao T, Qian L. 5-methyl-1H-benzotriazole as an effective corrosion inhibitor for ultra-precision chemical mechanical polishing of bearing steel. J Electrochem Soc 2020;167(13):131502.
[43] Deng C, Jiang L, Qian L. Synergistic effect of F− and persulfate in efficient titanium alloy chemical mechanical polishing. ECS J Solid State Sci Technol 2021;10(11):114003.
[44] Tang W, Zhang L, Chen Y, Zhang H, Zhou L. Corrosion and strength degradation behaviors of binderless WC material and WC–Co hardmetal in alkaline solution: a comparative investigation. Int J Refract Metals Hard Mater 2017;68:1–8.
[45] Kerkhof F, Moulijn JA, Heeres A. The XPS spectra of the metathesis catalyst tungsten oxide on silica gel. J Electron Spectrosc Relat Phenom 1978;14(6):453–66.
[46] Shi Y, Jin Z, Jiang G, Liu Z, Zhou Z. Wang Z. Electrochemical corrosion of YG15 cemented carbide. J Chin Soc Corrosion Protect 2019;39(3):253–9.
[47] Wang J, Zhou Y, Qiao Z, Goel S, Wang J, Wang X, et al. Surface polishing and modification of Ti-6Al-4V alloy by shear thickening polishing. Surf Coat Technol 2023:129771.